Build-to-Cost Architecture Wavefront Error Performance

Keck Adaptive Optics Note 644

R. Dekany, C. Neyman, P. Wizinowich, E. McGrath, C. Max

March 10, 2009 (DRAFT v4)

Contents

1 Introduction

In response to the 'build-to-cost' directive pursuant to the NGAO conceptual design review (held in April 2008), we have revised the NGAO system architecture, reducing system costs while continuing to provide outstanding science improvement on top-priority science cases.

This KAON begins with a review of the new architecture parameters, which are used as input to the Wavefront Error Budget Tool previously utilized to estimate NGAO performance.

2 Recent changes to the Wavefront Error Budget Tool

Note, subsequent to the April 2008 conceptual design review, this tool has undergone some expansion, most notably the implementation of a separate error budget to predict the sharpening of the furthest off-axis of three natural low-order wavefront sensor (LOWFS) stars. In addition, several minor bug fixes have been implemented (most notably a previous error in the atmospheric transmission for off-zenith targets), as well as a revision of the LGS tomography error terms based upon recent and extensive LAOS simulations performance by C. Neyman[1]. In general, we believe the level of tomography error for NGAO to be less than reported as the 'conservative assumptions' in KAON 429.

[1] See results posted at: http://www.oir.caltech.edu/twiki_oir/bin/view/Keck/NGAO/LGSAsterismStudy

3 New Baseline LGS Architecture

The new baseline LGS architecture that we have arrived at based on the elimination of a deployable integral field unit instrument is the following:

- A fixed LGS asterism consisting of one on-axis LGS and three fixed LGS symmetrically located on a radius, R. The optimal value of R is to be determined from the analysis (see Section 5.1). This "3+1" asterism is used for laser tomography over the science field. A total of 50W of laser power will be distributed uniformly between these four LGS.
- Three movable or point-and-shoot (PnS) LGS to be used to sharpen the three natural guide stars used to provide tip-tilt information (one will also be used for focus, astigmatism and high order low bandwidth information). These LGS are used as part of single LGS AO systems. A total of 25W of laser power will be distributed uniformly between these three LGS.

In addition to the LGS architecture change (with respect to the system design) the optics bench architecture has changed such that the 2nd relay is in transmission (as opposed to reflection) after the 1st relay. The LOWFS are fed by pickoff arms that would vignette the science field if guide stars are selected which are within the science field. This approach also precludes using the science object as a guide star.

4 Architecture Details Modeled

4.1 Launch Facility and LGS Return Assumptions

- All LGS are center launched
- Uplink tip-tilt only on each LGS WFS
- 100 ph/cm^2/sec/W in mesosphere
- Sodium column density: 3x10^9 atoms/cm^2
- Transmission from the laser out of the launch telescope = 0.75
- Atmospheric transmission[2] = 0.896 (at zenith)

4.2 LGS Wavefront Sensor Assumptions

- Telescope + AO system transmission to the LGS WFS = 0.39
- 4x4 pix/subap
- CCID56 (1.6 e⁻ RON[3], 0.80 QE589 , dark: 400 cnt/sec, 0.25 pix charge diffusion)
- 50% moon, some fratricide
- All "3+1" LGS wavefront sensors have the same, optimized integration time.
- All PNS LGS wavefront sensors have the same, optimized integration time (different than the "3+1" LGS WFS).
- "3+1" asterism radius should be fixed at the optimal value (likely ~10" radius).
- PNS LGS are movable about a 60" radius field.

4.3 Low Order Wavefront Sensor Assumptions (LOWFS)

- Telescope + AO system transmission to the LOWFS = 0.32
- 2 TT + 1 TTFA
- Single LGS AO – sharpened
- J+H band
- no ADC
- FoR diameter: 120"
- 32 x 32 MEMS DM
- H2RG (4.5e⁻ RON, 0.85 QEJ)

[2] Krisciunas et al., PASP **99,** 887 (1987).
[3] The actual noise model for the CCID56 is RON = 0.0007 * (frame rate) + 1.0125 e-

4.4 Seeing Conditions

Four seeing assumption cases were defined based on Mauna Kea data:

- Challenging or 37.5th percentile – r_0 = 14 cm, θ_0 = 2.15”
- Median or 50th percentile – r_0 = 16 cm, θ_0 = 2.7”
- Good or 62.5th percentile – r_0 = 18 cm, θ_0 = 2.9”
- Excellent or 87.5th percentile – r_0 = 22 cm, θ_0 = 4.0”

4.5 Science Cases to be Evaluated

The following science cases should be used to evaluate and optimize the NGAO performance.

1. Galaxy assembly & star formation history
2. Nearby Active Galactic Nuclei
3. Measurements of GR effects in the Galactic Center
4. Imaging & characterization of extrasolar planets around nearby stars
5. Multiplicity of minor planets

The primary driver for the first science case is IFU science of small faint objects. In this case we are interested in optimizing and determining ensquared energy.

All four of the other science cases are interested primarily in high Strehl (from the perspective of this analysis). In these cases we are interested in optimizing and determining the high order rms wavefront error and the tip-tilt error.

Sky coverage is important for four of the key science drivers. It would be useful to have some plots of low order (tip-tilt) error versus sky coverage for these cases.

The following table lists the relevant parameters that should be used for the key science drivers.

	Galaxy Assembly	**Nearby AGNs**	**Galactic Center**	**Exo-planets**	**Minor Planets**
Zenith angle (deg)	30	30	50	30	30
Guide stars	Field stars	Field stars	IRS 7, 9, 12N[4]	Field stars[5]	Field stars
NGS color	M	M	n/a	M	M
Required sky coverage	30%	30%	n/a	30%	30%
Galactic latitude(deg)	30	30	n/a	10	30
Science filter	K	Z	K	H	Z
Max science exposure time (sec)	1800	900	60 (image) 900 (spectra)	300 (TBC)	120

[4] For the record, we note that our analysis of the Galactic Center case does not deal explicitly with the issues of blind mode reconstruction from the 3 specific stars listed here. It should be possible to consider the specific blind mode errors using the TMT sky coverage tools maintained by Lianqi Wang. Due to the great brightness in H-band of IRS7, the tip-tilt error for Gal Center is always quite small.

[5] The assumption for now is that the parent star is not available as a LOWFS reference due to limitations on the ability to share science and LOWFS light.

For the purpose of the Galactic Center analysis the targets in the following table can be used as guide stars. There are many other potential guide stars available as can be seen in the Galactic Center H-band image in the OOCD and Blum et al. (ApJ 470: 864). The offsets in the table are relative to Sgr A* ($\alpha = 17^h 45^m 40.045^s$, $\delta = -29^o 00' 27.9''$). Note that these three stars are all variable by more than 1 magnitude, but they are so bright that this should not be a problem.

#	IRAS ID	J	H	K	Δα from Sgr A* (arcsec)	Δδ from Sgr A* (arcsec)
1	IRS 7	13.8	9.3	6.7	0.04	5.58
2	IRS 9	15.0	11.0	8.5	-3.86	12.91
3	IRS 12N	15.5	11.4	8.6	5.42	12.60

5 System Performance

5.1 Optimal 3+1 Asterism Radius

LAOS simulations describing the tomography error term under different asterisms were performed to understand the potential cost savings. Because one of the key build-to-cost decisions made early was to lower the priority of a wide-field deployable integral field spectrograph (d-IFS), we were able to concentrate solely on performing the best tomography on axis. In this way we have been able to separate the problem into the on-axis performance and the required sharpening of the natural low-order wavefront sensor (LOWFS) guide stars.

Through these analyses[6], we determined that the leading choice of 3+1 science asterism radius is 10”. The evaluation contours of tomography error (alone) for a 10 arcsec-radius 3+1 asterism is shown in Figure 1.

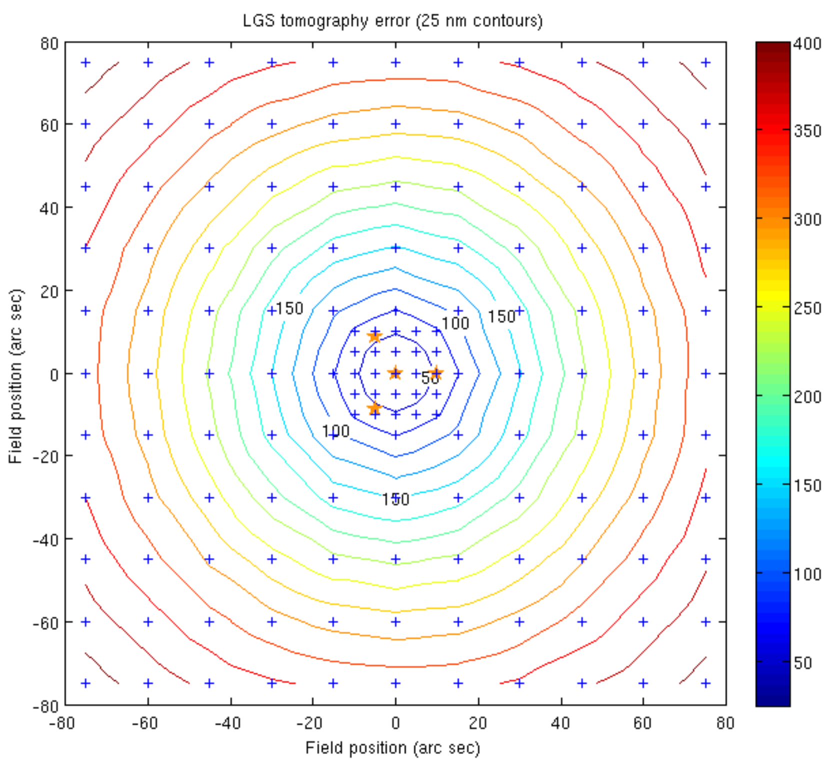

Figure 1 Tomography error for a 10”-radius 3+1 (or “Tetrad”) asterism.

[6] See http://www.oir.caltech.edu/twiki_oir/bin/view/Keck/NGAO/LGSAsterismStudy.

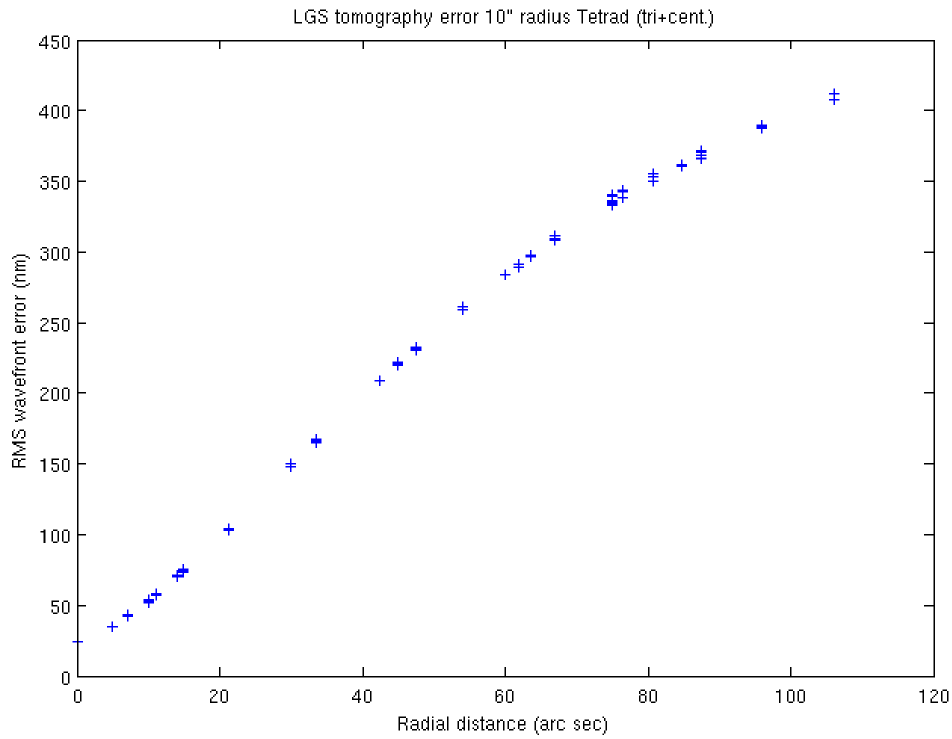

Figure 2 Tomography error for a 10”-radius 3+1 (or “Tetrad”) asterism.

Use of a 10”-radius 3+1 asterism was determined to be better than the next largest radius we studied, 20”. Although we cannot conclude at this time that a 10”-radius is better than at 15”-radius, we have proceeded to use a 10”-radius for the remainder of this report and recommend 10” as the baseline radius pending additional analysis of a 15” asterism and other considerations (see Section 5.9 below).

5.2 Sensitivity to Science Asterism Laser Power for fixed N = 64 subapertures

In order to understand the sensitivity of science case performance to science asterism laser power, we evaluated the performance of the system, holding the number of subapertures fixed at N=64 across. In the following section, we allow the optimum number of subaperture to vary. The results are shown in Figure 3.

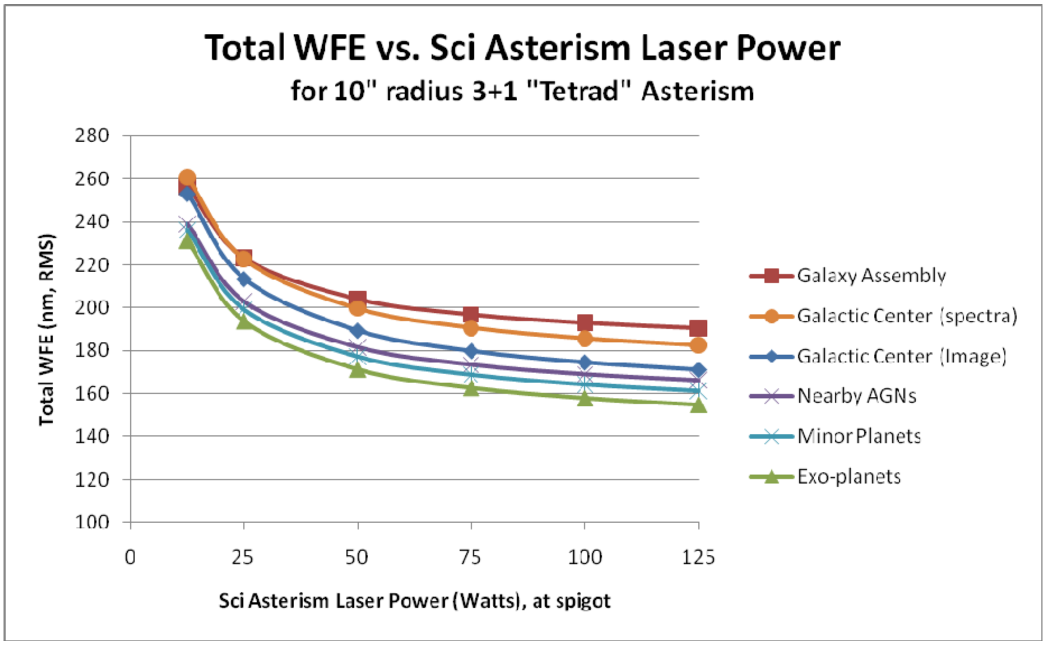

Figure 3 Residual RMS Wavefront Error (WFE) vs. Science Asterism Laser Power, as measured at the output of the lasers. The new baseline assumes 50W of science asterism power (with 25W of additional 'point and shoot' laser power not contributing to the high-order science wavefront measurement.)

This same curve can be interpreted in two additional ways. First, if our assumption of photo-return from the sodium layer is proven incorrect, the impact can be scaled from these curves directly. Similarly, if the sodium column density in the mesosphere on a given night is not 3×10^9 cm^{-2}, the photo-return can be scaled down (or up) depending on prevailing conditions.

The Strehl ratios corresponding to this same data are shown in Figure 4.

5.3 Performance vs. Sky Coverage Fraction

The sky coverage fraction and corresponding tip-tilt wavefront error for the key science cases is shown in **Figure 5**. We find that the assumption of independent PnS AO loops on the LOWFS NGS provides excellent performance over large sky fraction.

For 90% sky coverage, at the b=30 degrees galactic latitude assumed here (b=10 for the exoplanet case), a patrol range for the LOWFS of just about 60" was sufficient. We suggest further exploring sky fraction at higher galactic latitude in a separate study, using all the refinements to our tomography, transmission, and WFE budget models, which will also be relevant for the required patrol range (and unvignetted FoV of the 1st stage optical relay of NGAO).

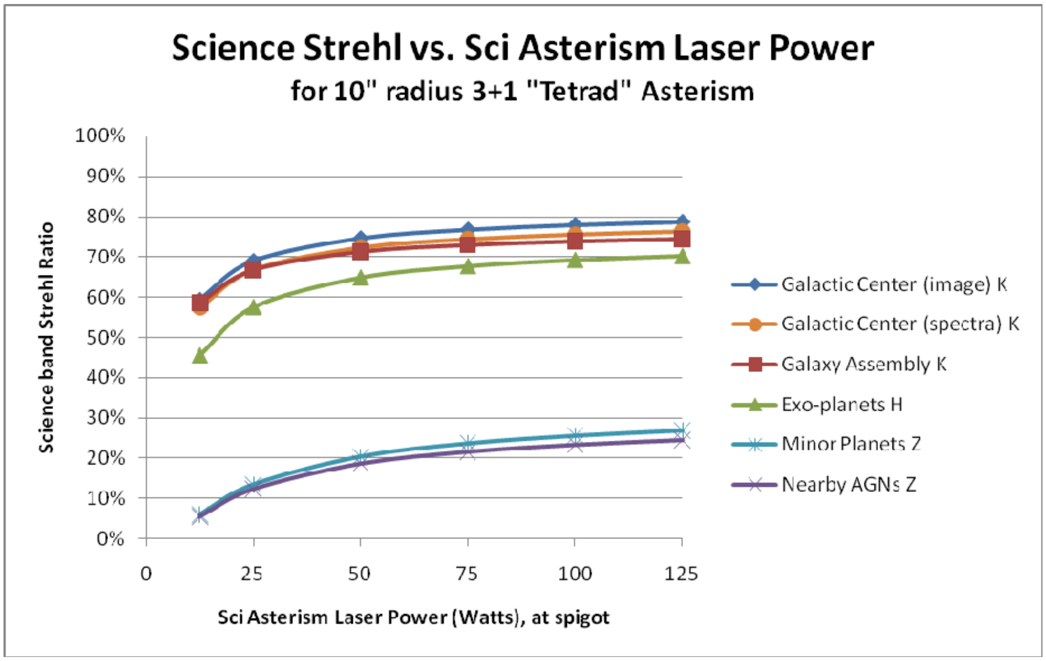

Figure 4 Strehl ratios corresponding to the performance in **Figure 3**, in the science band for each respective key science case.

5.4 Sensitivity to Seeing Conditions

The performance of NGAO will be a function of the ambient natural seeing conditions. The dependency of each respective science case performance metric on Fried parameter, r_0, is shown in Figure 6. On this curve, median conditions of r_0 = 16cm corresponds to approximately 0.6 arcsec FWHM seeing, while r_0 values of 0.08 and 0.22 correspond to ~1.2 arcsec and ~0.45 arcsec FWHM seeing, respectively.

5.5 Optimum Number of Pupil Subapertures (Average Sodium Column Density)

We explore the NGAO design performance and subsystem flow-down requirements as a function of available laser power put into the fixed 3+1 science asterism in Figure 7.

From these results, we see that for our baseline 50W of science asterism laser power, the optimum subaperture sampling for the cases considered is about N=56 for the assumed average sodium abundance of 3 x 10^9 cm^{-2}. However, we note that the penalty of using N=64, which would be preferred from an analysis of the NGAO high-contrast error budget, not considered here, is quite small for average sodium abundance. This can be seen in Figure 8, where the upper pair of curves indicate the performance form the Galaxy Assembly science case using the optimal number of subapertures and N=64 subapertures. In the regime of 50W of sodium laser power, using the optimal N=58 with optimal HOWFS sample rate of 912 Hz, results in a Strehl ratio less than 1% better than using the non-optimal N=64 with correspondingly optimized HOWFS sample rate of 870 Hz.

5.6 Optimum Number of Pupil Subapertures (Low Sodium Column Density)

If we further investigate the dependency of the optimum number of subapertures under particularly low sodium abundance, 1 x 10^9 cm^{-2}, we find the somewhat different results shown in Figure 8. Given the similar behavior between science cases observed in Figure 7, we only present the results for the Galaxy Assembly science case for clarity.

In this case, the optimum for 50W is seen to be about N = 46. However, one can further explore what specifically is the penalty of using a fixed pupil sampling, say N = 64, instead of the optimum sampling, assuming that the HOWFS frame rate can be changed to reoptimized in every case. The results of just this comparison are shown in **Figure 9**. We see that the penalty of using a fixed N = 64 subaperture sampling is quite small, even under conditions of low sodium abundance.

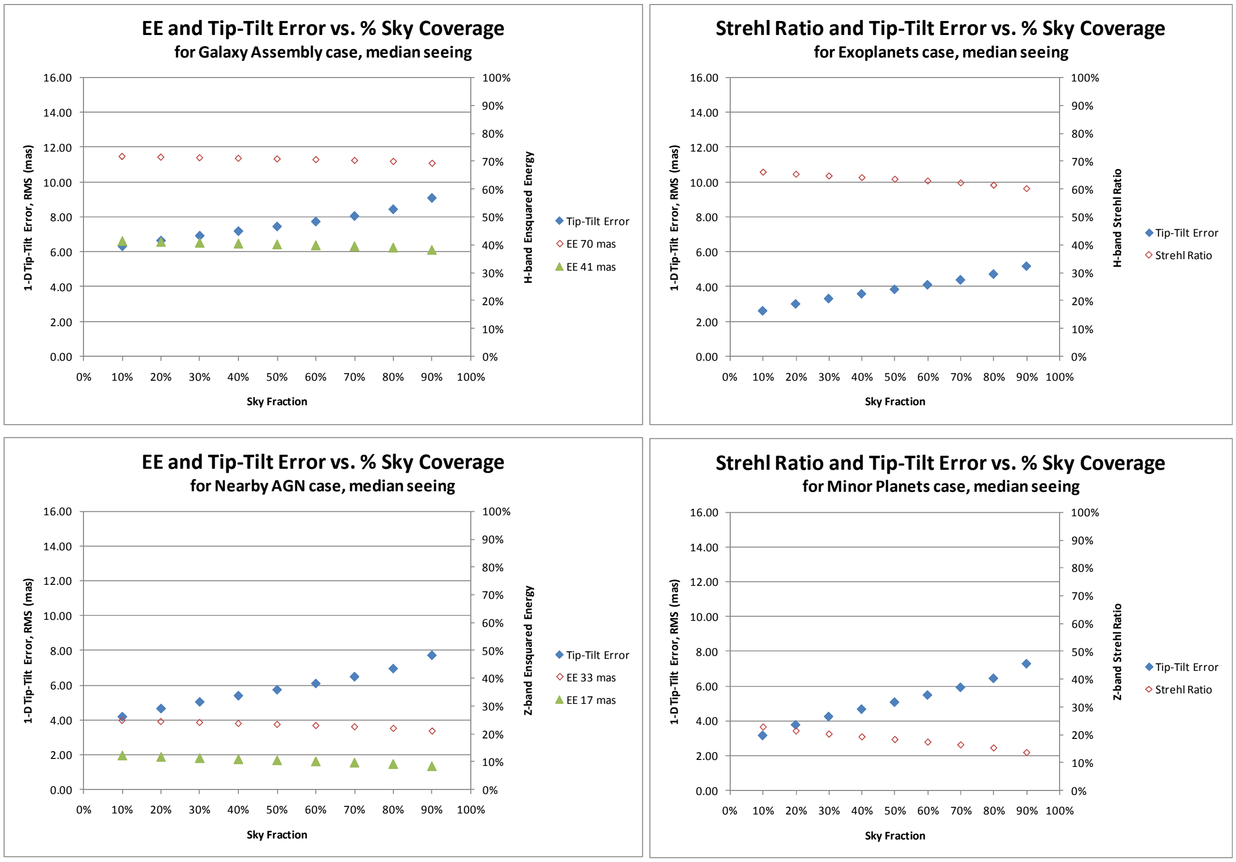

Figure 5 Science performance metrics for various sky coverage fractions with NGAO.

We conclude, therefore, that the optimum for number of subapertures across the pupil is quite shallow in the vicinity of our baseline architecture. This alone, however, is probably not sufficient argument to baseline only a single lenslet sampling in the HOWFS. For example, under conditions of light cirrus clouds, the photoreturn could be degraded further than considered here, in which case larger than 17cm (N=64) subapertures would likely be important to maintaining performance.

By similar argument, the performance penalty incurred by utilizing, say N = 56 subapertures, under conditions having optimal sampling of N = 64, is likely to be quite small. (Note, independent of the pupil sampling, having N = 64 actuators across the 2nd stage DM definitely benefits performance if we assume that all actuators can be used to compensate for static high-spatial-frequency wavefront errors.)

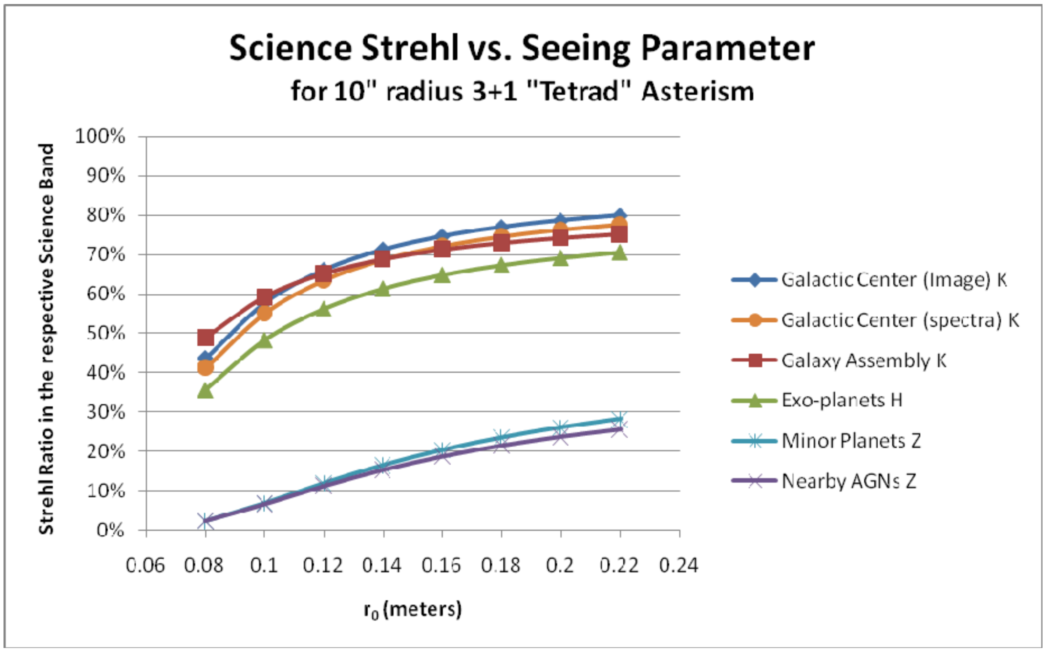

Figure 6 Science performance metrics for various seeing conditions.

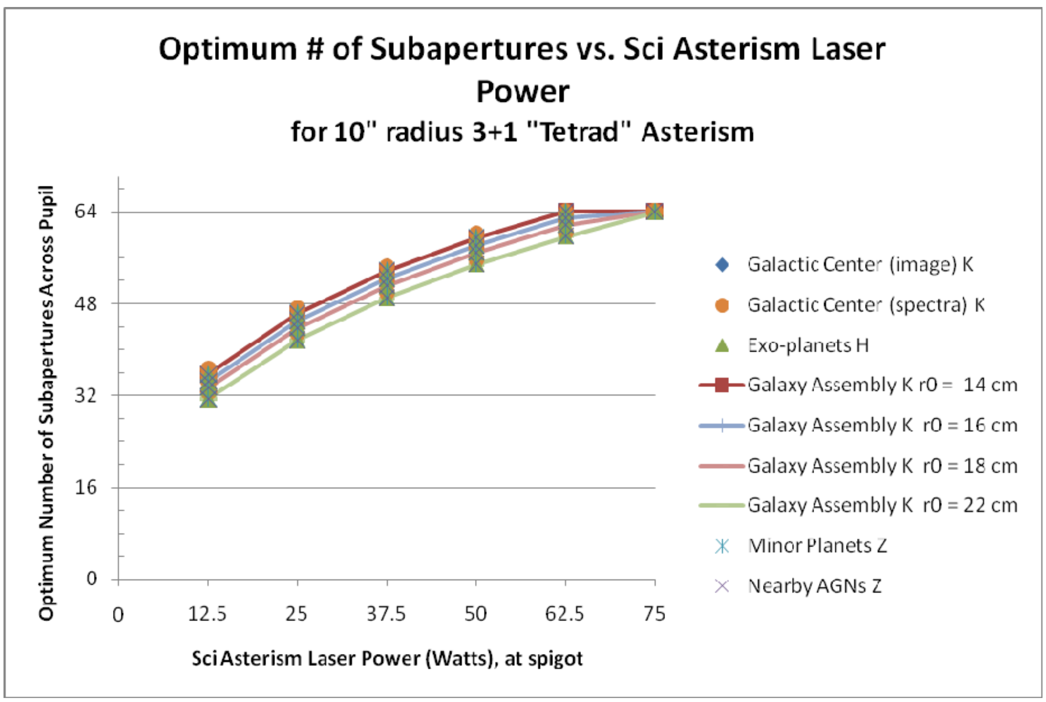

Figure 7 Optimum number of subapertures across the telescope pupil (10.949 m), for a variety of science cases. (Note the change in laser power scale compared to **Figure 3**.) Also shown here are optimal subaperture curves for the Galaxy Assembly case under 4 different seeing conditions (values of r_0).

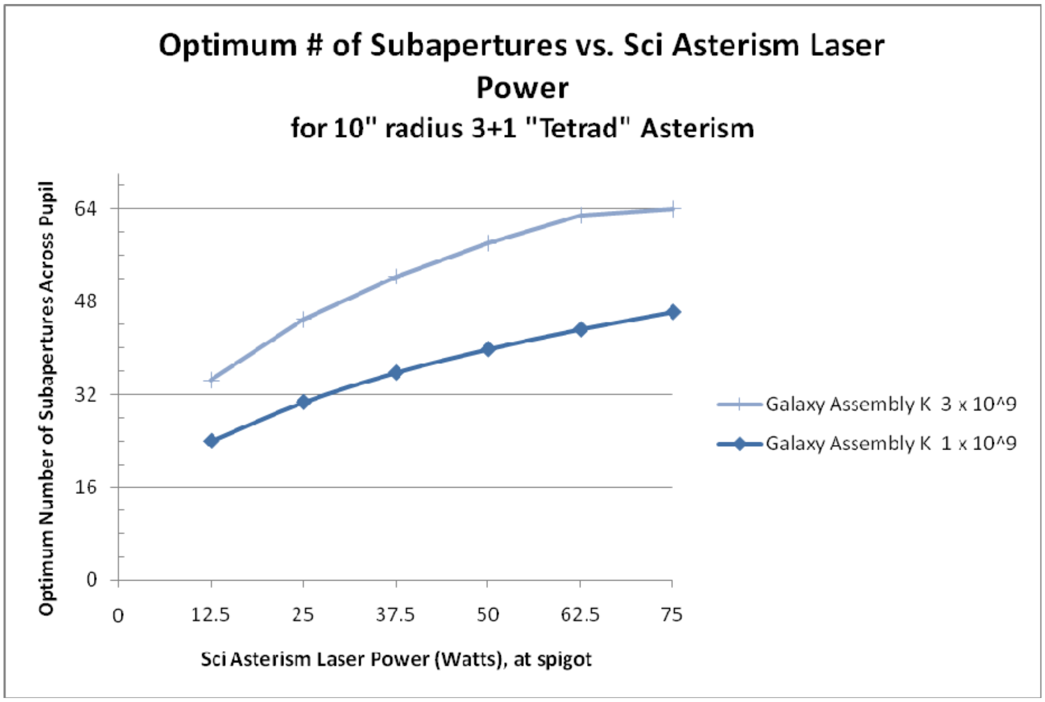

Figure 8 Optimum number of subapertures across the telescope pupil (10.949m), under average and low sodium column density conditions in median seeing conditions.

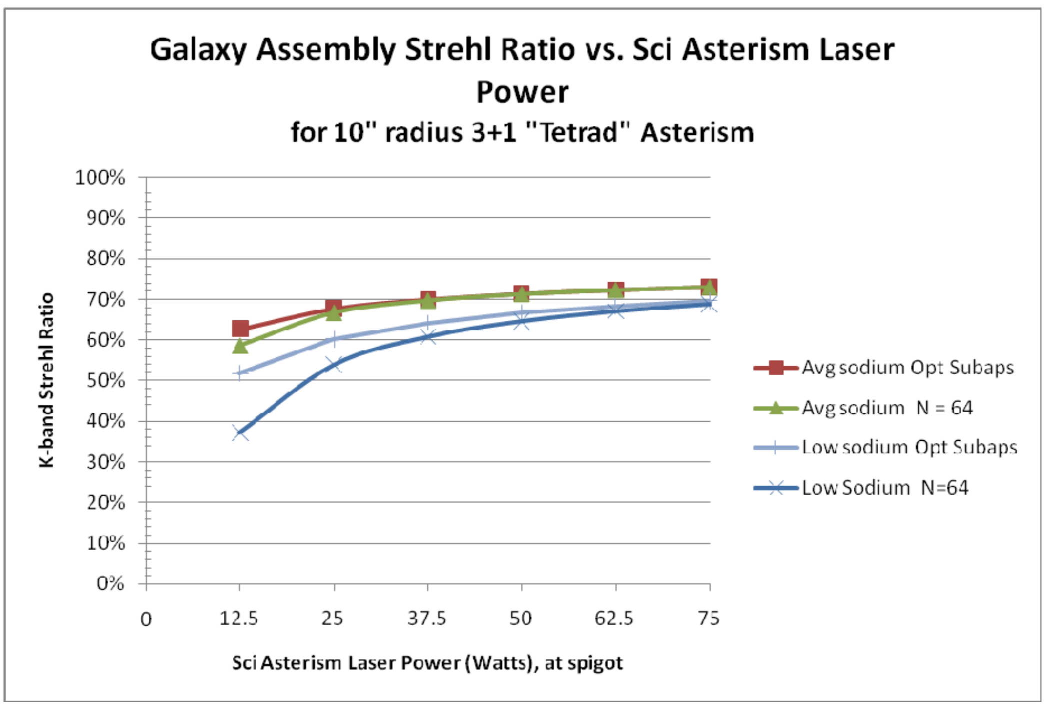

Figure 9 Strehl ratio for optimum and fixed number of subapertures for average and low sodium column density conditions. For our baseline 50W science asterism system, the error in K-band Strehl is always < 2%.

5.7 Anisoplanatism Across the Galactic Center Field of View

Using the assumptions described here, we have also analyzed the field performance for the Galactic Center science case, as shown in **Figure 10**. With the NGAO MOAO science path architecture, the best performance is typically applied to the center of the science field, with natural anisoplanatic fall-off for any finite off-axis distance.

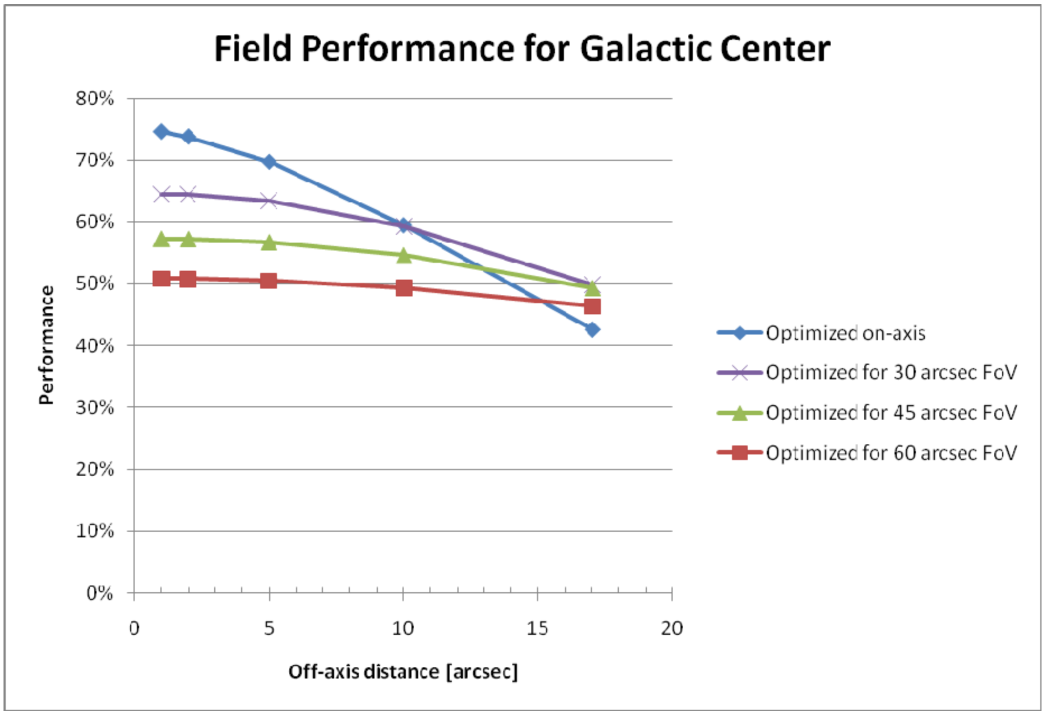

Figure 10 Strehl ratio vs. off-axis position for the Galactic Center science case, for MOAO control laws that optimize the correction for different fields of view. The correction on-axis can be traded off against better correction at the edge of the FoV. (The data here follow the single DM generalized anisoplanatism term shown in KAON 452.)

5.8 Low-order Wavefront Sensor Patrol Range

In regions of lower natural guide star density, e.g. toward the galactic pole, we must use low-order wavefront sensor (LOWFS) stars that are increasingly off-axis in order to optimize NGAO performance. For the best performance over the largest sky fraction, we find that patrol fields of regard (FoR) of as large as ~200" would be formally required. However, given the cost savings of reducing the unvignetted field of view of the NGAO optical relay, it is appropriate to ask what is the impact of restricting the LOWFS FoR on a typical science case.

We considered the impact of restricting the LOWFS FoR for the Galaxy Assembly science case to either 150" diameter or 120" diameter. We chose to evaluate the impact on K-band Strehl ratio as a function of desired sky coverage fraction (which might typically be determined by the nature of the specific survey undertaken), at galactic latitudes of b = 10 deg, b = 50 deg, and b = 90 deg. The results are shown in **Figure 10**.

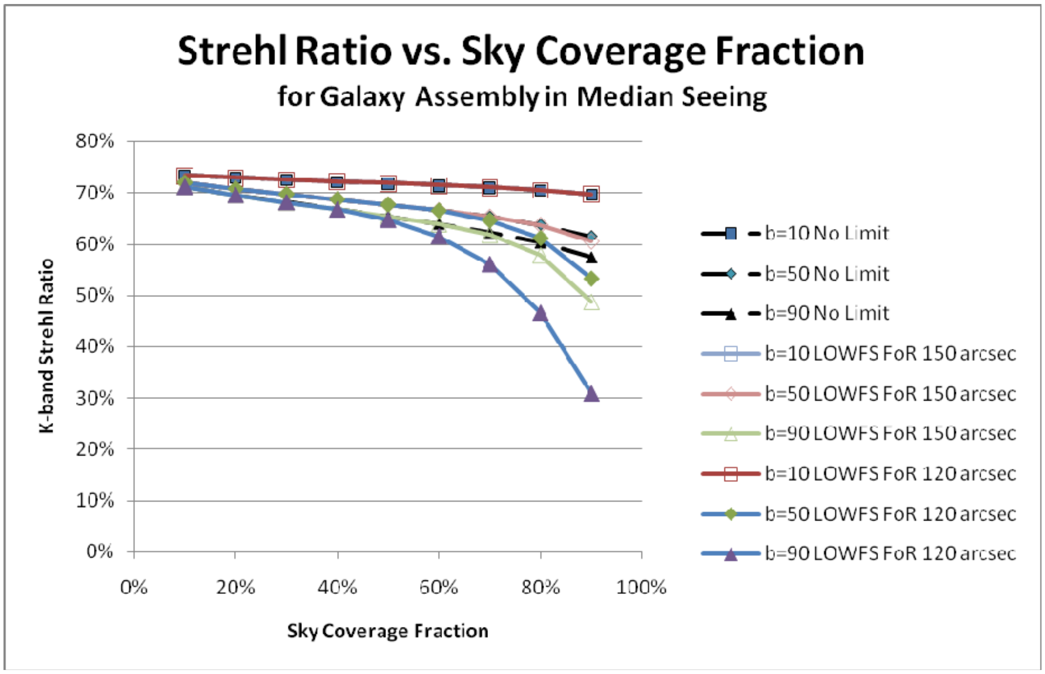

Figure 11 Performance impact of restricting the low-order wavefront sensor (LOWFS) patrol field of regard (FoR) for the Galaxy Assembly science case at different galactic latitudes, b.

We see that for the case of low galactic latitude (b=10 degrees), there is no penalty at all restricting the LOWFS FoR to either 150" or 120" (all curves with 'box' markers overlap near the top of **Figure 10**.) In fact, the shallow degradation in performance for any required sky fraction indicates that for b=10 there are plenty of field stars for NGAO to utilize.

For the case of b=50 degrees (shown on the curve with 'diamond' markers), the impact of 150" FoR is barely discernable, while that of 120" FoR amounts to a few % Strehl loss, starting above 70% sky fraction.

At the galactic pole, b = 90 degrees, the impact of restricting the FoR is greater. For 150" FoR, the impact can be as large as 10% Strehl reduction at high sky fraction, while for 120" FoR the impact can be a dramatic 30% reduction in K-Strehl. In both cases, the divergence from the performance of an unrestricted FoR begins at about 50% sky fraction.

The actual LOWFS NGS brightness and off-axis distance determined, statistically, using our Spagna infrared star brightness models is for the Galaxy Assembly case and a 120" LOWFS FoR limit is shown in **Figure 12**. For b=10, sky coverage can be increased through modest parallel increases in brightness and off-axis distance, never exceeding mV = 20 and about 45 arcsec off-axis. For b=50 and b=90, however, the limit of patrol range causes the brightness of available stars to fall more rapidly.

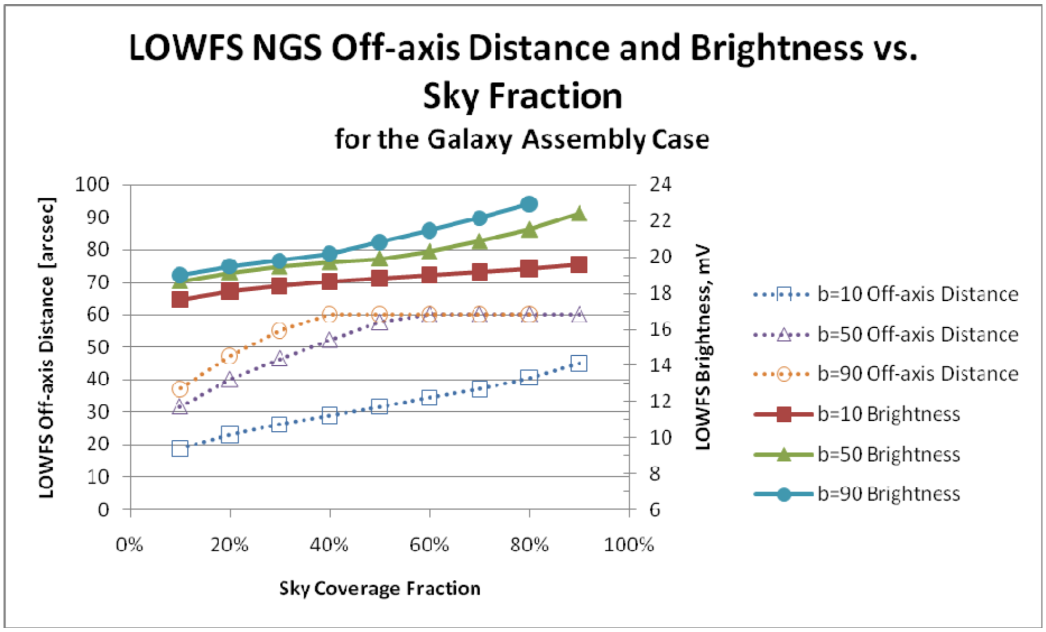

Figure 12 LOWFS NGS brightness and off-axis distance as a function of sky coverage fraction for the Galaxy Assembly science case. The off-axis distance here is limited to 60" corresponding to a (vignetting-limited) LOWFS FoR of 120" diameter. For this analysis we limit our brightest at mV = 23 and do not consider the challenges associated with acquiring such a sharpened LOWFS NGS.

Although this analysis is somewhat biased by the choice of K-Strehl as a metric (which is generally more forgiving of residual tip-tilt errors than shorter wavelength metrics) it still seems to us that the benefit of cost savings from requiring only a 120" unvignetted field of view through the NGAO first stage relay outweighs the potential impact on performance. In other words, it is only at high galactic latitude and high required sky coverage fraction, where performance will be substantially degraded. As none of our key science drivers has imposed these conditions upon NGAO, we shall proceed with the 120" field of view requirement.

5.9 Alternative 5+1 Asterism

A different approach to sharpening of our low-order wavefront sensor (LOWFS) natural guide stars (NGS) is the use of an entirely fixed, larger-radius diameter LGS asterism. If comparable in performance, this approach would have the benefit of foregoing the complexity of the patrolling 'point and shoot' LGS systems, saving mechanisms both on the uplink laser system and the selection of LGS by the HOWFS. Without the point and shoot subsystems to provide wavefront information in the direction of the LOWFS NGS, however, one has to rely upon MOAO correction using wavefronts estimated from the science asterism alone. This forces the science asterism to open to larger radius than would otherwise be required.

This approach furthermore trades off the potential benefit of utilizing all 75W of available sodium laser power in the calculation of the on-axis science correction with the increase in tomography error arising from use of a wider-distributed science asterism.

We investigated the tomography error performance of asterisms having one central LGS and 5 additional LGS on a regular pentagon of different radii, looking for the best trade between on-axis (science direction) tomography error and off-axis (MOAO-corrected LOWFS) tomography error. The best of these appears to be for a 40"-radius 5+1 asterism. The corresponding tomography error contour map is shown in **Figure 13** with the same data in radial plot format in **Figure 14**. We find that the on-axis tomography error of the 40" 5+1 asterism is about 36 nm RMS, while that of the 10" 3+1 asterism is ~23nm RMS. Although relatively small in the context of the overall wavefront error budget, this difference results in the on-axis science performance to be slightly better for the 10" 3+1 asterism using point and shoot sharpening.

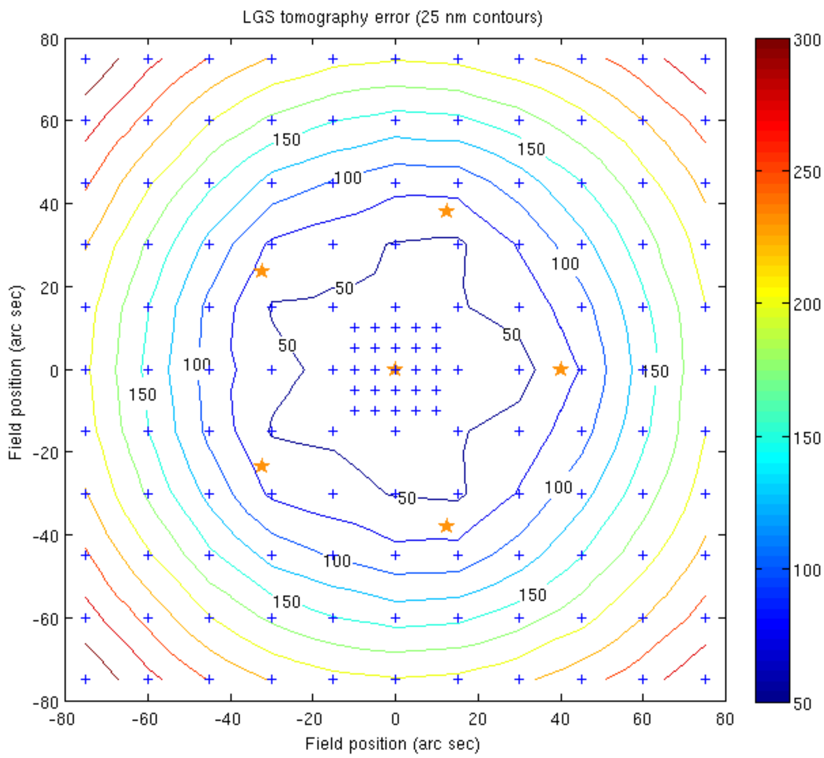

Figure 13 Tomography error for a 40”-radius 5+1 asterism.

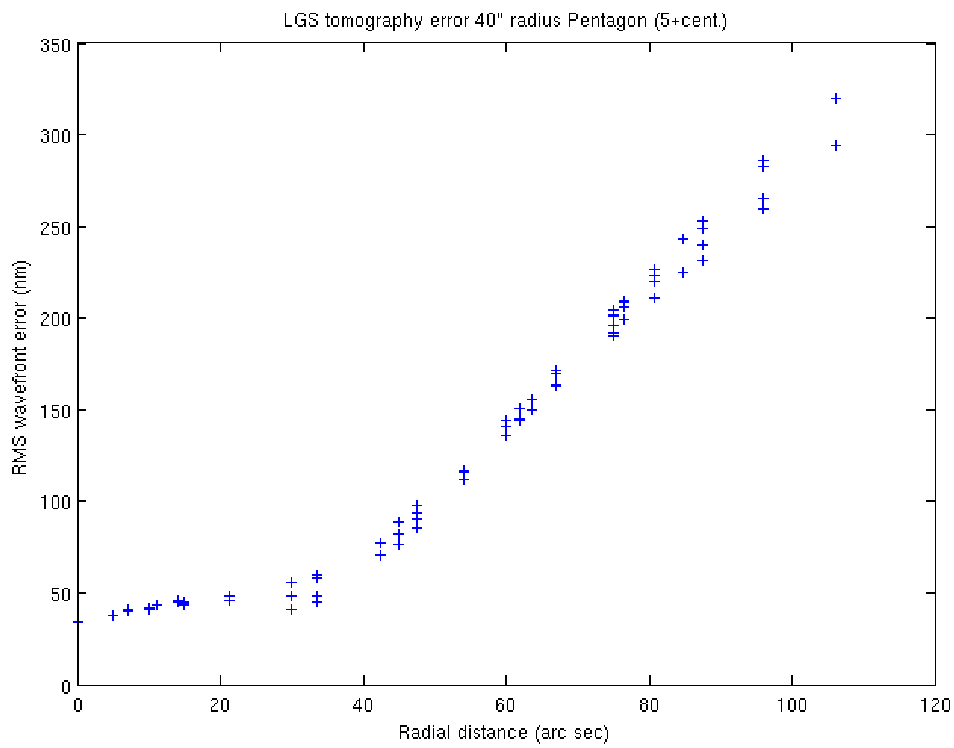

Figure 14 Tomography error for a 40”-radius 5+1 asterism.

In terms of LOWFS NGS sharpening, the determination of which of the fixed 40” 5+1 asterism or the 10” 3+1 asterism with point and shoot provides better correction is a function of the typical off-axis distance of the LOWFS NGS, which in turn depends on the required sky coverage fraction and galactic latitude. The effect of this can be seen in **Figure 15**.

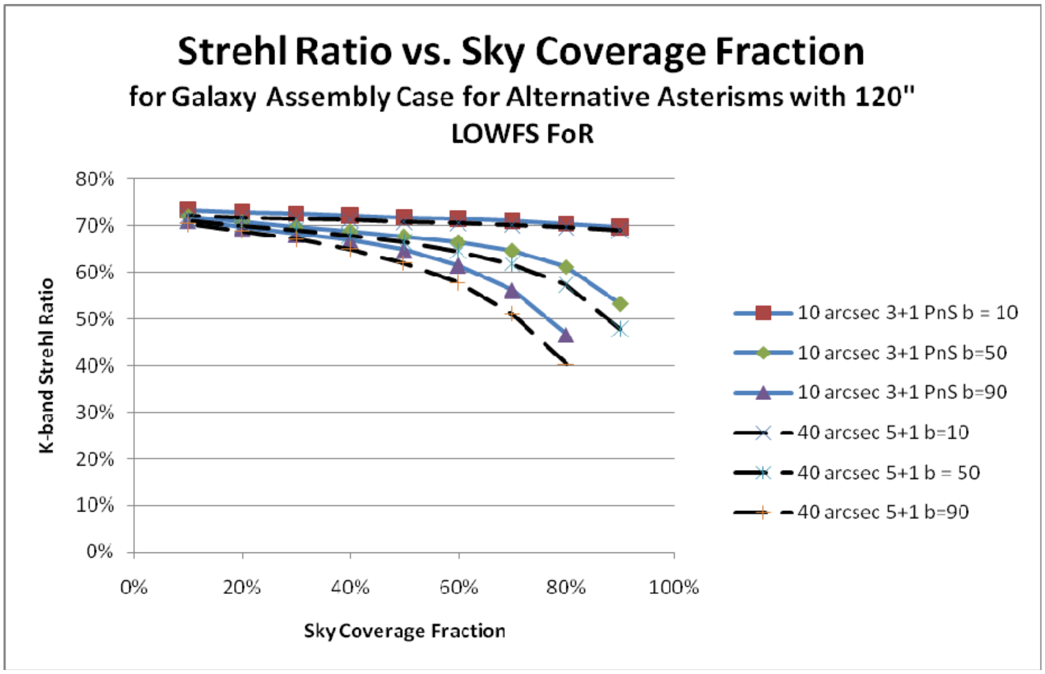

Figure 15 Performance comparison of an alternative fixed 5+1 laser asterism on 40” radius and a fixed 3+1 laser asterism on 10” radius, with the addition of 3 patrolling ‘point and shoot’ laser guide stars running independent LGS AO loops for the purpose of low-order wavefront sensor natural guide star sharpening. This data is for a 120” LOWFS FoR and LOWFS mV limit of 23 (and thus sky fraction above 80% is not possible to obtain at the galactic pole.)

We see that for low galactic latitude (b = 10 degrees) the Galaxy Assembly case K-band Strehl ratio is not limited by the residual tip-tilt error, so that the benefit of the lower LOWFS tomography error for the 40” 5+1 asterism does not overcome the small on-axis science tomography benefit of the 10” 3+1 asterism with point and shoot. As the LOWFS NGS move further off-axis (for higher sky fraction), the advantage of lower 5+1 tomography error begins to compensate some of the on-axis tomography degradation, but never seems to quite overcome it. At large off-axis LOWFS distance (particularly when compared to the 40” 5+1 asterism radius), the LOWFS MOAO tomography error grows, so that in none of the cases considered here does the 40” 5+1 asterism outperform the 10” 3+1 asterism with PnS. (Whether the loss of performance shown here is acceptable to realize the cost savings of the fixed 5+1 asterism will not be considered here.)

A similar plot, without the limitation of 120” LOWFS FoR, showing the stronger benefit for the point and shoot concept at high galactic latitude and sky fraction is shown in
Figure 16. In this case, the rapid increase in MOAO tomography error for far-off-axis LOWFS NGS with the 40” 5+1 asterism leads to an even more distinct advantage for the PnS system.

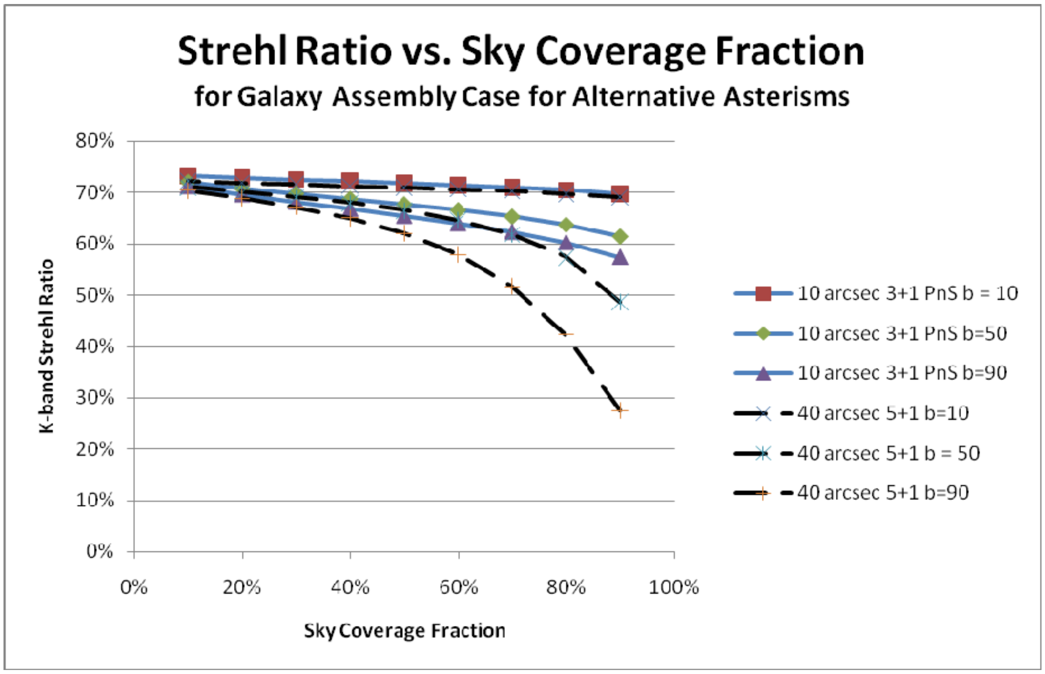

Figure 16 Performance comparison of an alternative fixed 5+1 laser asterism on 40" radius and a fixed 3+1 laser asterism on 10" radius, with the addition of 3 patrolling 'point and shoot' laser guide stars running independent LGS AO loops for the purpose of low-order wavefront sensor natural guide star sharpening. Here LOWFS NGS are selected as necessary to strictly satisfy the sky coverage fraction indicated with a brightness limit of mV = 23 (e.g. NGS up to about 100" off-axis, where the 5+1 asterism MOAO LOWFS tomography error greatly exceeds the focal anisoplanatism error of the point and shoot AO systems.)

These analyses assumed completely independent PnS AO systems. Of course, at the cost of additional computing complexity, the PnS approach allows the option of integrating wavefront information from both the science asterism *and* the point and shoot LGS tomographically to provide even better NGS sharpening. We suggest this be the basis for a separate trade study in conjunction with the RTC design team.

6 Example Output from WFE Budget Tool

For reference, we include three portions of the v1.43 WFE Budget Tool that was used for this analysis. Note, certain functionality, notably detailed Truth WFS photometry (and error budget) is not yet implemented.

Model			
AO System	NGAO LGS	*HO Error*	*162*
Sci. Case	Exo Jup LGS	*TT Angular Error*	*3.3*
Sci. Instr.	*TBD*	*Total Effective Error*	*171*

				Global Parameters	x	x	x	x	x	x	
Worksheet	**Parameter**	**Current Parameter Value**	**Units**		**Gal Cen**	**Gal Cen Spectra**	**Exo Jup LGS**	**KBO**	**Galaxy Assembly**	**Nearby AGN**	**NGAO LGS**
Telescope	Name	Keck									Keck
Atm	Dec				-30	-30		-12			20
	Zenith angle	30.0	deg		Dec	Dec	30	Dec	30	30	
	Cn2(h) model	Mauna Kea Ridge									Mauna Kea Ridge
	r0	0.160	m								0.160
	Wind speed	9.5	m/s								9.5
	Outer scale	50	m								50
HO Flux	Guide star spectral type	LGS	(NGS/LGS)		LGS	LGS	LGS	LGS	LGS	LGS	
	Guide star brightness	LGS	mV								
	HOWFS NGS color	LGS									
	Num LGS subaps	64									64
	Num NGS subaps	0									
	HO Integration time	0.00115	sec								
	HOWFS detector	CCID56									CCID56
LGS Flux	Na column density	3E+09	atoms/cm^2	3E+09							
	Pulse format	CW									CW
	Laser power	50.00	Watts								50.0
	Return source	Measured	(Measured/Theoretical)	Measured							
	Laser-thru-LLT projection transmission	0.75									0.75
HO Cent	Num pix per subap	4									4
	Pixel IFoV	1.6	arcsec								1.6
	Range Gating?	NO									NO
	Intrinsic HOWFS GS diameter	0.0	arcsec		LGS	LGS	LGS	LGS	LGS	LGS	0.0
	Perfect uplink AO?	NO									NO
	Aberrations in uplink	0.9	arcsec								0.90
	LLT off-axis distance	0.0	m								0.0
	Use max LGS elongation?	NO		NO							
	AO system aberrations	0.25	arcsec								0.25
	Charge diffusion	0.25	pixels								0.25
	ADC in HOWFS?	NO									NO
FA Tomo	Number of laser beacons	4									4
	LGS beacon height (km) above telescope	90.00									90
	LGS asterism radius	0.17	arcmin								
	Single laser backproj FA reduction factor	0.8									0.8
Na H	Max vertical velocity of Na layer	30.0	m/s	30.0							
Fit	Physical actuator pitch	0.0035	m								0.004
Alias	Use anti-aliasing in HOWFS?	NO									NO
	Aliasing reduction factor	0.67		0.67							
Stroke	Number of Woofer actuators across the pupil	64									64
	Number of Tweeter actuators across the pupil	0									0
	Woofer PV stroke	4.0	microns								4.0
	Tweeter PV stroke	0.0	microns								0.0
	Available Woofer interactuator stroke	1.0	microns								1.0
	Available Tweeter interactuator Stroke	0.0	microns								0.0
	Woofer conjugate height	0.0	meters								0.0
	Tweeter conjugate height	0.0	meters								0.0
	Static surface errors to be corrected	0.7	microns								0.7
Go-To	Science Mode	MOAO	(SCAO/MOAO/MCAO)								MOAO
Dig	Number of controller bits	16	bits								16
TT Flux	TT Guide star brightness	18.42	mV		12.20	12.20					
	TT NGS color	M			IRS7	IRS7	M	M	M	M	
	Subaperture type	circular	(circular/square)	circular							
	Num TT used for tip/tilt	2									2
	Num TTFA used for tip/tilt	1									1
	Num 3x3 used for tip/tilt	0									0
	Num HOWFS used for tip/tilt	0									0
	TT Integration Time	0.0041	sec								
	TT compensation mode	Indep PnS	(SCAO/MOAO/MCAO/MOAO Point and Shoot,Indep PnS)								MOAO Point and Shoot
	TT detector	H2RG									H2RG
TT Meas	Sensor type	SH	(Pyramid/SH)								SH
	Is TT star sharpened by AO?	YES									YES
	Assume Fermenia TT sharpening	NO		NO							
	ADC in TT sensor?	NO									NO
	Num pix per subap	2									2
	Binning factor	1									1
	Pixel IFoV (for background calc)	0.02	arcsec								0.015
	Intrinsic TT GS diameter	0.0	arcsec		0.0	0.0	0.0	0.00	0.00	0.00	
TWFS Flux	TWFS Guide star brightness	10.00	mV		12.2	12.2	13.0				
	TWFS NGS color	M			IRS7	IRS7	M	M	M	M	
	Number of TWFS subaps per pupil	5									5
	Integration Time	10.0000	sec								
	TWFS compensation mode	SCAO	(SCAO/MOAO/MCAO)								SCAO
	TWFS detector	CCID56									CCID56
Bandwidth	Kappa	1.0									1.0
	HO servo decimation factor	20									20
	TT servo decimation factor	20									20
	Telescope input tip/tilt reduction	0.25									0.3
	LGS Focus Sensor	TWFS	(TWFS/TT)								TWFS
	TWFS Integration Time	0.5	sec								0.500
Aniso	Optimize LGS off-pointing	NO		NO							
	HO GS to Target for Sci Aniso WFE	1.00	arcsec		1.0	2.0	1.0	0	1	1	
	HO GS to TT GS for TT Aniso WFE	25.27	arcsec		5.6	5.6					
	TT GS to Target (for TT Anisoplanatism)	26.27	arcsec		5.6	5.6					
	TWFS GS to Target (for Truth Anisoplanatism	25.00	arcsec		5.6	5.6					
CA	CA rejection factor	10.00									10
Atm Dispersion	Sci dispersion correction (ADC)?	YES									YES
	Correction factor	20		20							
Cal	Instrument	TBD			TBD	TBD	TBD	TBD	TBD	TBD	
	Uncorrectable AO system aberrations	30	nm								30
	Dynamic WFS Zero-point Calibration Error	40	nm								40
	Leaky Integrator Zero-point Calibration Error	15	nm								15
	DM-to-pupil misregistration error	25	nm								25
	DM-to-lenslet pupil scale error	15	nm								15
Sky Coverage	TT Star density model	Spagna		Spagna							
	Required sky coverage fraction	30%			N/A	N/A	30%	30%	30%	30%	
	TWFS Star density model	Bachall		Bachall							
	Required TWFS sky coverage fraction	*30%*									
	Galactic latitude (b in deg)	10			0	0	10	30	30	30	
Science Filter	Science Filter	H			K	K	H	Z	K	Z	
	Max Sci Exp Time (sec)	300			60	900	300	120	1800	900	
					Gal Cen	**Gal Cen Spectra**	**Exo Jup LGS**	**KBO**	**Galaxy Assembly**	**Nearby AGN**	

Figure 17 WFE budget tool v1.44 Input Summary Sheet for these analyses.

Keck Wavefront Error Budget Summary

Version 1.44

Mode: **NGAO LGS**
Instrument: **TBD**
Sci. Observation: **Exo Jup LGS**

Science Band	u'	g'	r'	i'	Z	Y	J	H	K
λ (μm)	0.36	0.47	0.62	0.75	0.88	1.03	1.25	1.64	2.20
δλ (μm)	0.06	0.14	0.14	0.15	0.12	0.12	0.16	0.29	0.34
λ/D (mas)	6.7	8.8	11.6	14.1	16.6	19.4	23.5	30.8	41.4

Science High-order Errors (LGS Mode)		Wavefront Error (rms)	Parameter
Atmospheric Fitting Error		48 nm	64 Subaps
Bandwidth Error		59 nm	**43 Hz (-3db)**
High-order Measurement Error		77 nm	50 W
LGS Tomography Error		37 nm	**4 sci beacon(s)**
Asterism Deformation Error		22 nm	0.50 m LLT
Chromatic Error		2 nm	Upper limit
Dispersion Displacement Error		2 nm	Estimate
Multispectral Error		25 nm	30 zen; sci wav
Scintillation Error		20 nm	0.34 Scint index, J-band
WFS Scintillation Error		10 nm	Alloc
	121 nm		
Uncorrectable Static Telescope Aberrations		43 nm	64 Acts
Uncorrectable Dynamic Telescope Aberrations		40 nm	Dekens Ph.D
Static WFS Zero-point Calibration Error		25 nm	Alloc
Dynamic WFS Zero-point Calibration Error		40 nm	Alloc
Leaky Integrator Zero-point Calibration Error		15 nm	Alloc
Stale Reconstructor Error		15 nm	Alloc
Go-to Control Errors		38 nm	Alloc
Residual Na Layer Focus Change		34 nm	30 m/s Na layer vel
DM Finite Stroke Errors		0 nm	4.0 um P-P stroke
DM Hysteresis		13 nm	from TMT model
High-Order Aliasing Error		16 nm	64 Subaps
DM Drive Digitization		1 nm	16 bits
Uncorrectable AO System Aberrations		30 nm	Alloc
Uncorrectable Instrument Aberrations		30 nm	TBD Instrument
DM-to-lenslet Misregistration		15 nm	Alloc
DM-to-lenslet Pupil Scale Error		15 nm	Alloc
	107 nm		
Angular Anisoplanatism Error		16 nm	1.0 arcsec
Total High Order Wavefront Error	161 nm	**162 nm**	**High Order Strehl**

Strehl Ratio (%)	u'	g'	r'	i'	Z	Y	J	H	K
High Order Strehl	0.00	0.01	0.07	0.16	0.27	0.39	0.52	0.69	0.81

Science Tip/Tilt Errors	Sci Filter	Angular Error (rms)	Equivalent WFE (rms)	Parameter
Tilt Measurement Error (one-axis)		1.46 mas	25 nm	18.4 mag (mV)
Tilt Bandwidth Error (one-axis)		1.30 mas	22 nm	10.9 Hz (-3db)
Tilt Anisoplanatism Error (one-axis)		2.18 mas	37 nm	**26.3** arcsec from sci
Residual Centroid Anisoplanatism		1.10 mas	19 nm	10 x reduction
Residual Atmospheric Dispersion	*H*	0.26 mas	5 nm	20 x reduction
Induced Plate Scale Deformations		0.00 mas	0 nm	0 m conj height
Science Instrument Mechanical Drift		0.42 mas	7 nm	Alloc 5 mas / hr
Long Exposure Field Rotation Errors		0.83 mas	14 nm	Alloc 10 mas / hr
Residual Telescope Pointing Jitter (one-axis)		0.49 mas	8 nm	29 Hz input disturbance
Total Tip/Tilt Error (one-axis)		**3.3 mas**	61 nm	**Tip/Tilt Strehl**
Total Effective Wavefront Error			**171 nm**	**Total Strehl (%)**

Strehl ratios (%)	u'	g'	r'	i'	Z	Y	J	H	K
Tip/Tilt Strehl	0.45	0.59	0.71	0.79	0.84	0.87	0.91	0.95	0.97
Total Strehl (%)	0.00	0.00	0.05	0.13	0.23	0.34	0.48	0.65	0.79
FWHM (mas)	7.5	9.4	12.1	14.5	16.9	19.7	23.8	31.0	41.6

Spaxel / Aperture Diameter (mas)		31	62	50	70	90	180	240	480	1100		36
Ensquared Energy	*H*	Square	0.37	0.65	0.59	0.68	0.69	0.72	0.74	0.80	0.85		0.50

Sky Coverage Galactic Lat. 10 deg

Corresponding Sky Coverage	**30.0%**	This fraction of sky can be corrected to the Total Effective WFE shown

Assumptions / Parameters

					LGS power	50 W at laser(s)	Excitation (all LGS 90km)		2478 ph/cm^2/sec
r0	**0.147 m**	**at this zenith**	Wind Speed	11.0 m/s	Zenith Angle	30 deg			
Theta0_eff	**2.14 arcsec**	**at this zenith**	Outer Scale	75 m	HO WFS Rate	870 Hz	SH	using	CCID56
Sodium Abund.	3×10^9	atoms/cm^2	LGS Ast. Rad	0.17 arcmin	HO WFS Noise	1.6 e- rms			
Science AO Mode:	MOAO		HOWFS Tran	0.35	HOWFS anti-aliasing	NO			
LOWFS AO Mode:	Indep PnS				HOWFS transmission	0.35			
LOWFS Star Type:	M	Num TT 2	Num 3x3 0		LO WFS rate	243 Hz	SH	using	H2RG
Max Exposure Time	300 sec	Num TTFA 1	Num HOWFS 0		LO WFS Noise	4.5 e- rms			
Max mechanical tip/tilt rejection bandwidth		100 Hz			LOWFS transmission	0.32			

Figure 18 Example science WFE budget for the Exoplanets Case.

Keck LOWFS Wavefront Error Budget Summary

Version 1.44

Mode:	**NGAO LGS**
Instrument:	**TBD**
Sci. Observation:	**Exo Jup LGS**

Science Band	u'	g'	r'	i'	Z	Y	J	H	K
λ (μm)	0.36	0.47	0.62	0.75	0.88	1.03	1.25	1.64	2.20
δλ (μm)	0.06	0.14	0.14	0.15	0.12	0.12	0.16	0.29	0.34
λ/D (mas)	7	10	13	15	18	21	26	34	46

LOWFS High-order Errors (Mode)	**26.3** arcsec off-axis	**Wavefront Error (rms)**	**Parameter**	
Atmospheric Fitting Error		85 nm	32	Acts Across
Bandwidth Error		59 nm	43	Hz (-3db)
High-order Measurement Error		75 nm	8.3	W
LGS Tomography Error		150 nm		SCAO
Asterism Deformation Error		22 nm	0.50	m LLT
Chromatic Error		2 nm		Upper limit
Dispersion Displacement Error		2 nm		Estimate for IR TT
Multispectral Error		25 nm	30	zen; flux-wght wav
Scintillation Error		20 nm	0.34	Scint index, J-band
WFS Scintillation Error		10 nm	Alloc	
	201 nm			
Uncorrectable Static Telescope Aberrations		59 nm	32	Acts Across
Uncorrectable Dynamic Telescope Aberrations		40 nm		
Static WFS Zero-point Calibration Error		25 nm	Alloc	
Dynamic WFS Zero-point Calibration Error		40 nm	Alloc	
Leaky Integrator Zero-point Calibration Error		15 nm	Alloc	
Stale Reconstructor Error		15 nm	Alloc	
Go-to Control Errors		0 nm	Alloc	
Residual Na Layer Focus Change		34 nm	30	m/s Na layer vel
DM Finite Stroke Errors		15 nm	1.5	um P-P MEMS strok
DM Hysteresis		2 nm	from LAO	
High-Order Aliasing Error		16 nm	64	Subaps
DM Drive Digitization		1 nm	16	bits
Uncorrectable AO System Aberrations		53 nm	Alloc	
Uncorrectable Instrument Aberrations		30 nm	TBD	Indep PnS
DM-to-lenslet Misregistration		15 nm	Alloc	
DM-to-lenslet Pupil Scale Error		15 nm	Alloc	
	117 nm			
Angular Anisoplanatism Error		0 nm	25.27	arcsec
Total High Order Wavefront Error	232 nm	**232 nm**	**High Order Strehl**	

Strehl Ratio (%)	u'	g'	r'	i'	Z	Y	J	H	K
High Order Strehl	0.00	0.00	0.00	0.02	0.07	0.14	0.26	0.46	0.65

Assumptions / Parameters

			Effective PnS GS radius	0.27 arcmin	LGS power	8.3 W at laser(s)	LGS return per beacon		348 ph/cm^2/sec
r0	0.147 m	at this zenith	Wind Speed	11.0 m/s	Zenith Angle	30 deg			
Theta0_eff	2.14 arcsec	at this zenith	Outer Scale	75 m	HO WFS Rate	869 Hz	SH	using	CCID56
Sodium Abund.	3 x 10^9	atoms/cm²	LGS Ast. Rad.	0.17 arcmin	HO WFS Noise	1.6 e- rms			
Science AO Mode:	MOAO		HOWFS Trans	0.35	HOWFS anti-aliasing	NO			
LOWFS AO Mode:	Indep PnS				HOWFS transmissio	0.35			
LOWFS Star Type:	M	Num TT 2	Num 3x3	0	LO WFS rate	243 Hz	SH	using	H2RG
Max Exposure Tim	300 sec	Num TTFA 1	Num HOWFS	0	LO WFS Noise	4.5 e- rms			
Max mechanical tip/tilt rejection bandwidth			100 Hz		LOWFS transmissio	0.32			

Figure 19 Example LOWFS NGS WFE budget for the Exoplanets Case.